Scientia Iranica B (2021) 28(6), 3216–3231

Sharif University of Technology
Scientia Iranica
Transactions B: Mechanical Engineering
http://scientiairanica.sharif.edu

Experimental study of heat transfer characteristics of nanofluid nucleate and film boiling on horizontal flat plate

S.H. Golkar, M. Khayat*, and M. Zareh

Department of Mechanical Engineering, Science and Research Branch, Islamic Azad University, Tehran, P.O. Box 14515-775, Iran.

Received 25 October 2020; received in revised form 1 January 2021; accepted 3 May 2021

KEYWORDS
Nucleate boiling;
Film boiling;
Critical heat flux;
Minimum heat flux;
Nanofluids.

Abstract. This study investigated the heat transfer characteristics of nanofluid nucleate and film boiling experimentally. To this end, Al_2O_3 and SiO_2 deionized water-based nanofluids were prepared with three volumetric concentrations of 0.1%, 0.3%, and 0.5%. Boiling experiments were conducted on a circular and polished copper surface with a diameter of 25 mm. The results illustrated that the addition of nanoparticles to the base fluid reduced the heat transfer coefficient of nucleate boiling. Boiling of nanofluids elevated surface wettability and the critical heat flux was significantly higher than that of pure deionized water. The Al_2O_3 deionized water-based nanofluid with a volumetric concentration of 0.5% had the best performance, with a critical heat flux of 44.56% higher than that of pure deionized water. The presence of nanoparticles in the deionized water-based nanofluid improved the heat transfer coefficient of film boiling. As demonstrated by the results, the stable film boiling for nanofluids began with a more significant difference in wall superheat temperature than pure deionized water. Among the investigated concentrations, the volumetric concentration of 0.5% yielded the best performance for both nanofluids such that the minimum heat fluxes of Al_2O_3 and SiO_2 deionized water-based nanofluids increased by 35.01% and 34.40%, respectively, compared to pure deionized water.

1. Introduction

Among various heat transfer methods, boiling phenomenon characterized by high thermal efficiency is widely used in various industries such as power plants, chemical industries, refrigeration, and air conditioning systems. In these industries, flat or curved surfaces are used horizontally, vertically, and inclined as boiling surfaces among which boiling on horizontal surfaces facilitates cooling electronic systems, heat exchangers, and boilers. The growing need for these industries and their high efficiency has led researchers to focus on the enhancement of cooling and heat transfer. The main problem with the use of boiling phenomenon lies in the high and uncontrolled temperature of heat transfer devices which limits the choice of materials in these devices. Reforms that promote the efficiency of these systems are of great significance to energy saving. Therefore, researchers have focused on methods for improving the boiling phenomenon for many years. Different techniques have been proposed to improve the boiling process, one of which is the addition of nanoparticles to the base fluid.

*. *Corresponding author. Tel.: +98 2144868536*
E-mail addresses: hadi.golkar@srbiau.ac.ir (S.H. Golkar); mkhayat@srbiau.ac.ir (M. Khayat); m.zareh@srbiau.ac.ir (M. Zareh)

doi: 10.24200/sci.2021.56967.4997

The results based on the dispersion of nanoparticles help engineers design an efficient thermal system [1]. The presence of nanoparticles in the base fluid can enhance some of the thermal and thermophysical properties of the fluid. In the pool boiling of nanofluids, the addition of nanoparticles to the base fluid increases the specific surface area. On the other hand, the Brownian motion of the nanoparticles increases the turbulence and mixing in the fluid, which leads to an increase in thermal conductivity. Because nanoparticles are primarily made of metals or metal oxides, they have higher thermal conductivity than base fluids. Therefore, coupling between nanoparticles increases the thermal conductivity of nanofluids by creating a chain of nanoparticles connected to each other that causes heat transfer to occur at a higher rate.

The advantages of nanofluids and the development of nanotechnology have led to use of nanofluids in the boiling process in many recent empirical studies. In the cooling of some industrial systems, heat transfer may take place in all boiling curve regions and cover a wide range of heat fluxes. For this reason, researchers have studied the two nucleate and film boiling regimes. Although some researchers have studied these two boiling regimes numerically [2–5], many studies have investigated them experimentally as well, to be reviewed below.

Shahmoradi et al. [6] conducted pool boiling experiments for water-alumina nanofluid with volumetric concentrations of less than 0.1% on a flat plate of copper. It was observed that by increasing the volumetric concentration from 0.01% to 0.1%, the heat transfer coefficient of nucleate boiling would be reduced and the Critical Heat Flux (CHF) would increase. The decrease in heat transfer coefficient of the nucleate boiling results from the deposition of nanoparticles in the boiling process and the filling of the nucleation sites. Besides, heat flux augmentation results from increase in surface wettability. Raveshi et al. [7] investigated the nanofluid pool boiling of a binary mixture of water-ethylene glycol and alumina at the same volume ratio on a flat plate of copper. It was found that there was an optimum volumetric concentration for nanofluids, which had the highest nucleate boiling heat transfer coefficient. The optimum concentration was 0.75% and the highest increase in nucleate boiling heat transfer coefficient was reported 64%, compared to base fluid.

Umesh and Raja [8] investigated the pool boiling of pentane-copper oxide nanofluid with volumetric concentrations of 0.005% and 0.01% on flat heaters of brass. It was observed that at low volumetric concentrations, the nucleate boiling heat transfer coefficient increased by 5% to 25% compared to the base fluid, but decreased upon increase in the nanofluid volumetric concentration. Ji et al. [9] conducted boiling experiments on water-silica nanofluid with mass concentrations of 0.025%, 0.05%, and 0.1% to investigate the effects of surface wettability on pool boiling. The results demonstrated that upon increasing the mass concentration from 0.025% to 0.1%, the nucleate boiling heat transfer coefficient decreased. The reason for this decrease was the deposition of nanoparticles on the boiling surface, which made the surface more hydrophilic and delayed the occurrence of nucleate boiling. Dareh et al. [10] conducted pool boiling experiments on pure water and water-alumina nanofluids with volumetric concentrations of 0.0025%, 0.005%, and 0.01% on the micro- and nano-structured surfaces. The results showed that for all the surfaces, the CHF of the nanofluid was higher than that of the base fluid.

Kiyomura et al. [11] investigated the pool boiling of a Fe_2O_3 water-based nanofluid at mass concentrations of 0.029 and 0.29 gr/lit on copper surface. The effects of nanoparticle deposition and surface roughness on contact angle, surface wettability, and heat transfer coefficient of nucleate boiling were investigated. The results illustrated that the highest nucleate boiling heat transfer coefficient belonged to the polished surface with a lower concentration of nanoparticles. Vasudevan et al. [12] investigated the pool boiling of reduced graphene oxide water-based nanofluid with volumetric concentrations of 0.2%, 0.6%, and 0.8% on a flat plate of copper. The results showed that the CHF increased following an increase in the volumetric concentration from 0.2% to 0.8%. It was observed that the CHF increase occurred due to the increase in bubble density and existence of small bubbles. Reddy and Venkatachalapathy [13] investigated the pool boiling of hybrid nanofluid (Al_2O_3-CuO/water) with different volumetric concentrations on a flat plate of copper. The results illustrated that the CHF of the hybrid nanofluid was higher than that of the single-type nanofluid. It was observed that by increasing the volumetric concentration from 0.01% to 0.1%, the nucleate boiling curves shifted towards the right side due to nanoparticle deposition, leading to enhanced capillary action.

Kamel and Lezsovits [14] conducted the pool boiling experiments on tungsten oxide water-based nanofluid with volumetric concentrations of 0.005%, 0.01%, and 0.05% on horizontal copper tube. It was observed that as the applied heat flux increased, the nucleate boiling heat transfer coefficient increased. The results demonstrated that by increasing the volumetric concentration from 0.005% to 0.05%, the nucleate boiling heat transfer coefficient decreased. Mohammadi and Khayat [15] conducted the pool boiling experiments on Al_2O_3 and CuO water-based nanofluids with a volumetric concentration of 0.1% on a flat plate of copper. The results showed that the CHF of the nanofluids was higher than that of the water. It was

found that the boiling of nanofluids on the microgroove surface could not be used for a long-term process due to the deposition of nanoparticles over time and the creation of an insulation layer on the surface.

Gylys et al. [16] presented experimental results of film boiling by testing the cooling process of spherical surfaces in subcooled water. Spherical surfaces are made of three different types of steel, copper, and aluminum. The results showed that the minimum film boiling temperature was influenced by the thermal diffusion characteristics of the surface (thermal conductivity, thermal capacity, and density), water temperature, and heat transfer rate between the surface and the liquid. Arai and Furuya [17] investigated the film boiling experiments by quenching a high-temperature stainless steel sphere in Al_2O_3 water-based nanofluid at volumetric concentrations of 0.024% to 1.3%. The film boiling heat transfer rate of nanofluid was reported to be approximately similar to, or slightly lower than, that of water. Ciloglu et al. [18] investigated the pool-film boiling of Al_2O_3, SiO_2, TiO_2, and CuO water-based nanofluids with a volumetric concentration of 0.1%. A high-temperature cylindrical rod was used as the boiling surface. The results showed that during iterative tests, the cooling time was reduced and the main reason was the change of the surface properties due to the deposition of nanoparticles on the surface.

Li et al. [19] conducted boiling experiments by quenching hot stainless steel spheres in the water-based nanofluid pool in the presence of carbon nanotubes (CNTs) of different sizes. The results demonstrated that due to differences in the size of the nanoparticles, the CHF and Leidenfrost point increased up to different values. The results of the contact angle and roughness test demonstrated that the porous layers affected surface roughness rather than surface wettability. Kang et al. [20] conducted film boiling experiments to evaluate the effects of surface hydrophobicity on minimum film boiling temperature and Minimum Heat Flux (MHF) by quenching the spherical surfaces of saturated water. Superhydrophobic surfaces were prepared by anodic oxidation on zirconium surface. The results showed that the superhydrophobic surfaces increased the minimum film boiling temperature and the MHF.

Wciślik [21] reviewed the effect of adding common nanoparticles to the base fluid on the Leidenfrost temperature and performed a simple economic analysis of the use of nanoparticles. Among the five nanoparticles investigated in this paper (Ag, Al_2O_3, SiO_2, TiO_2, and C-diamond), Al_2O_3 nanoparticles with a size of 39 nm and a volumetric concentration of 0.1% had the best thermal effect. In most of the analyzed cases, the minimum film boiling temperature is inversely correlated with the volumetric concentration of nanofluids. Talari et al. [22] investigated the effects of micro/nanostructured surfaces on the Leidenfrost drop temperature with an emphasis on its enhancement and discussed the mechanism of surface topology improvement. It was observed that multiscale surfaces significantly increased the Leidenfrost temperature and had a better performance by combining the benefits of both nano and micro structures.

A review of literature points to the larger number of nanofluid film boiling experiments conducted on spherical and cylindrical surfaces rather than on the horizontal flat plate. The occurrence of film boiling at high temperatures has limited its experimental study; therefore, the majority of boiling studies have focused on nucleate boiling. Due to the ability of our instrument to work at high temperatures, the present paper made it possible to conduct film boiling experiments on the horizontal flat plate. The experimental study of nanofluid film boiling on the horizontal flat plate is a new aspect of the present paper. However, to conduct more comprehensive studies, nucleate boiling is also investigated. To this end, the effects of adding nanoparticles to the base fluid on the nucleate and film boiling heat transfer coefficient, CHF, MHF, and minimum film boiling temperature are investigated experimentally.

2. Experimental apparatus and test procedure

2.1. Description of problem

In the present study, boiling experiments were carried out under the same laboratory conditions with ambient pressure of 80 kPa, ambient temperature of 23°C, and water boiling temperature of 92.9°C. Boiling experiments were applied to a circular and polished copper surface with a diameter of 25 mm. The fluids used for boiling experiments include pure deionized water and two types of Al_2O_3 (α) and SiO_2 deionized water-based nanofluids. To investigate the effects of nanofluid volumetric concentration on the heat transfer characteristics of film and nucleate boiling, experiments were carried out with three volumetric concentrations of 0.1%, 0.3%, and 0.5%.

2.2. Pool boiling experimental apparatus

A schematic of the pool boiling apparatus used in this study is shown in Figure 1. This device includes a structural part, retaining bases, and a test chamber. Data processing, lighting, power transmission, and heating parts are located in the lower section of the test chamber. The test chamber is a Pyrex glass with the diameter, height, and thickness of 200, 300, and 5 mm, respectively. In addition, to prevent heat dissipation, the outer part of Pyrex is coated with one layer of fiberglass, two layers of thermal insulation, and one layer of aluminum insulation glue. On the top of the Pyrex, there is a safety glass cover with dimensions of 400 × 400 mm and, in this cover, a pressure gauge

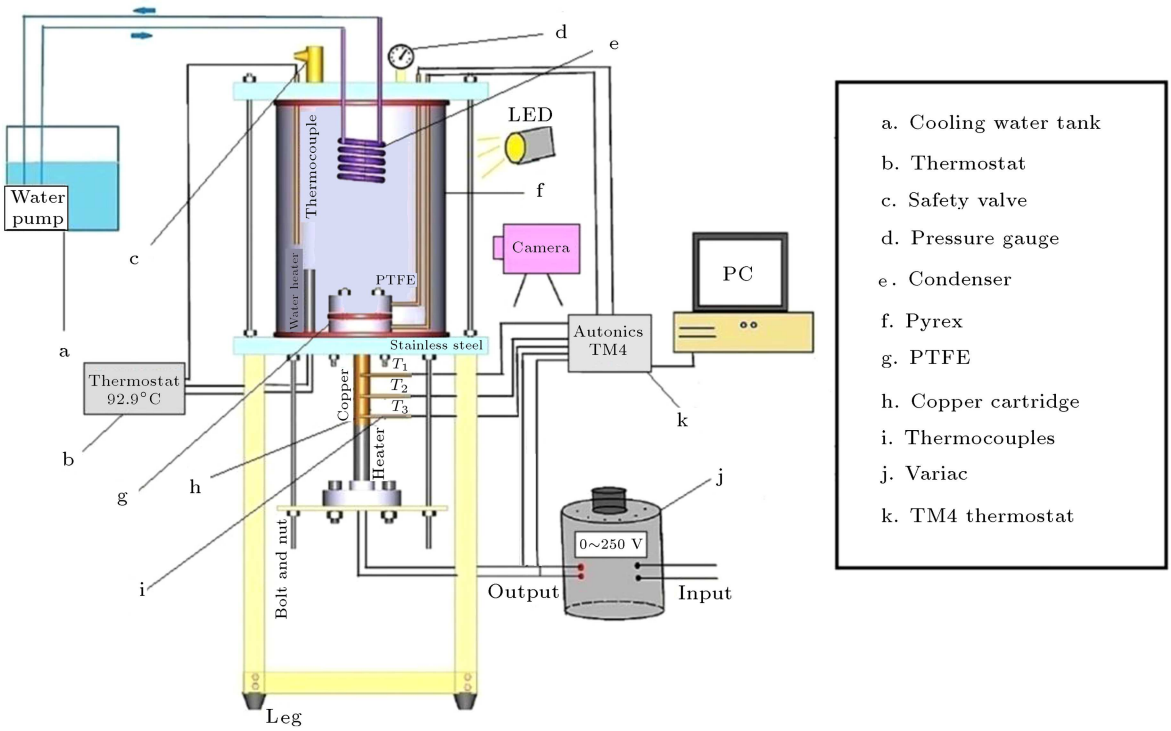

Figure 1. Pool boiling apparatus and its components in a schematic form.

and a safety valve are located. A pressure gauge was employed to display the pressure inside the test chamber which remained constant. The M-shaped rod pre-heater with a power of 500 W is located in the fluid to warm the operating fluid to its saturation temperature at atmospheric pressure before and during the test. A condenser with a diameter of 10 mm and a length of 15 cm was employed to cool and condense the water into the chamber and a pump with a discharge of 400 lit/hr was employed to keep the water inside the condenser continuously rotating.

Cartridge is a cylinder with two different cross-sections at top and base and is made of copper with a purity of 99%. Figure 2(a) and (b) show the copper cartridge before being placed in the pool boiling apparatus. The total height of the cartridge is 120 mm and the upper and lower section diameters are 25 mm and 140 mm, respectively. The upper cross-section is used as the boiling surface. On the upper neck of this cartridge, three holes are created with a diameter of 2 mm and a distance of 7 mm from each other and the thermocouples are located on them. In the bottom part of the cartridge cross-section, eight holes with a diameter of 10 mm and a depth of 55 mm have been created, which is the location of the heaters. In the present apparatus, a variance of 3000 W with a variable output of 0 to 250 V is used to power the device.

To record the temperatures of the three thermocouples connected to the cartridge and that of a thermocouple inside working fluid, a TM4-type thermostat was employed to record the data into the computer every second. Silicon paste was used to prevent heat dissipation in holes where heaters and thermocouples were located in cartridges. In addition, silicon glues

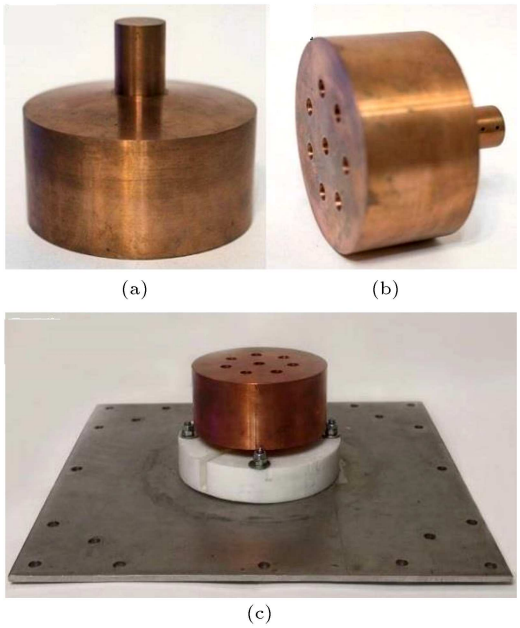

Figure 2. (a) and (b) Copper cartridge before being placed in the pool boiling apparatus, and (c) PTFE wrapped around the copper cartridge.

with high thermal resistance were used to seal Pyrex and its underlying steel as well as between the cartridge and Teflon thermal insulation (PTFE). Teflon thermal insulation is a circle with a diameter of 14 cm and a thickness of 3 cm. Figure 2(c) shows how the PTFE is wrapped around the copper cartridge. On the wall of this piece, three holes with a diameter of 3 mm were created to pass the thermocouples and they remained aligned with the location of the thermocouples on the cartridge. The thermocouples used in this device were of K type and covered a temperature range of −200°C to 1350°C.

To simplify the experiment procedure, the heat transfer in the cartridge is assumed to be one-dimensional; therefore, it is necessary to insulate the cartridge to prevent heat loss in the radial direction. Therefore, first, the cartridge is covered by glass wool with a thermal conductivity rate of 0.04 W/m.°C and temperature resistance of 750°C. Then, a layer of thick PTFE sheet is fastened to the glass wool. Then, another layer of glass wool and an elastomeric insulator are placed over the whole set and tightly closed.

2.3. Preparation of nanofluids

The nanofluids used in the boiling experiments of the present study include Al_2O_3 (α) and SiO_2 nanoparticles in deionized water-based fluid. In Table 1, the characteristics of the nanoparticles used in this study are presented.

Table 1. Specifications of nanoparticles.

Nanoparticles →	Al_2O_3 (α)	SiO_2
Producer	US NANO	Degussa
Color	White	White
Dimension (nm)	50	12
Density (gr/cm3)	3.97	2.24

To reach the volumetric concentrations of 0.1%, 0.3%, and 0.5% in a liter of deionized water, the required mass of each nanoparticle was calculated using Eq. (1). Table 2 shows the mass requirements of the nanoparticles at different volumetric concentrations:

$$m = \frac{\rho_{np} \times V_{nf} \times (\varphi \times 10^{-2})}{(1 - \varphi \times 10^{-2})}. \quad (1)$$

In Eq. (1), ρ_{np} is the nanoparticle density, V_{nf} nanofluid volume, and φ volumetric concentration.

Figure 3 shows a schematic of the nanofluid preparation process used in boiling experiments. For preparation of the nanofluids, a magnetic stirrer was used to distribute the particles into the base fluid. Also, an ultrasonic probe (UP400St, hielscher) with the power of 400 W and frequency of 24 kHz was used to stabilize the solution, and an ultrasonic bath tank (WUC-D10H, DAIHAN Scientific Co., Ltd) with the power of 665 W and frequency of 40 kHz was used to homogenize and remove the agglomerates.

To test the stability of nanofluids, the deposition of nanoparticles in the base fluid over time has been studied visually. For example, the nanofluid stability test with a volumetric concentration of 0.5% is shown in Figure 4(a) and (b). According to these figures, the deionized water-based Al_2O_3 and SiO_2 nanoparticles

Table 2. Required mass of nanoparticles at different volumetric concentrations.

Nanoparticles →	Al_2O_3 (α)	SiO_2 (gr)
Volumetric concentration of 0.1%	3.974	2.242
Volumetric concentration of 0.3%	11.945	6.740
Volumetric concentration of 0.5%	19.950	11.256

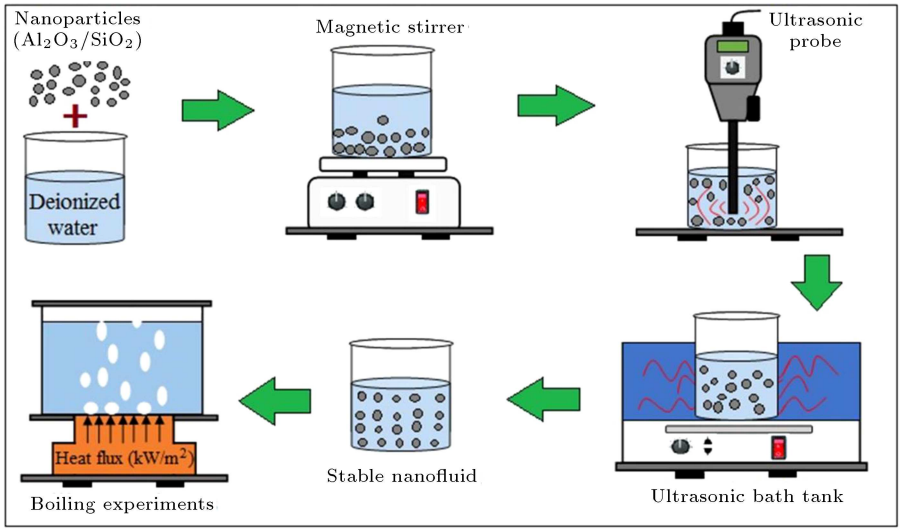

Figure 3. Schematic of preparation of nanofluids for boiling experiments.

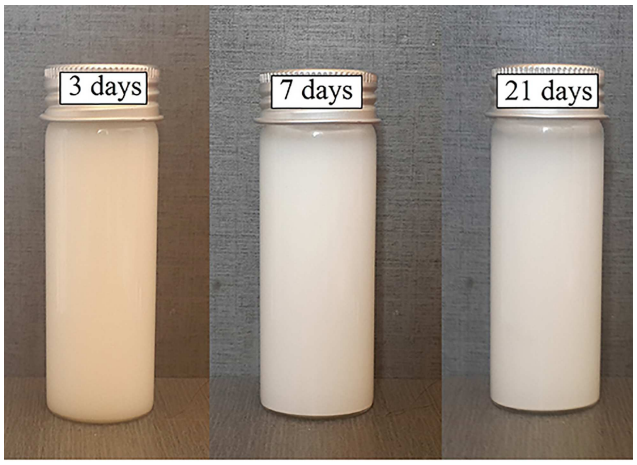

(a)

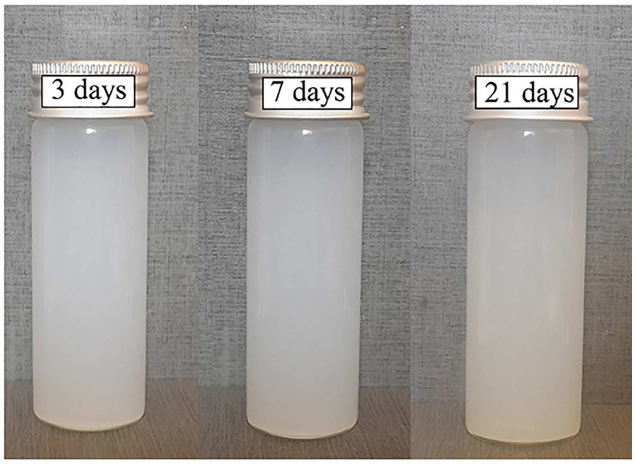

(b)

Figure 4. Deposition test of deionized water-based nanoparticles at a volumetric concentration of 0.5%: (a) Al_2O_3 and (b) SiO_2.

had good stability after 21 days. It is noteworthy that boiling experiments were performed one day after the preparation of nanofluids.

To investigate the size and shape of nanoparticles, Transmission Electron Microscopy (TEM) images of nanofluids were prepared. In Figure 5(a) and (b), the TEM images of Al_2O_3 and SiO_2 nanoparticles in deionized water-based fluid with a volumetric concentration of 0.5% are shown, respectively. According to these figures, the nanoparticles are well dispersed in the base fluid and the dimensions reported in the images are consistent with the stated dimensions.

2.4. Measurement and data error analysis

First, the Pyrex chamber is filled with one liter of working fluid and the pre-heater is turned on to warm up the water to the saturated temperature (92.9°C at 80 kPa). At this point, the condenser is turned on so that vapors condense and return to the boiling chamber. In the next step, the main heaters are switched

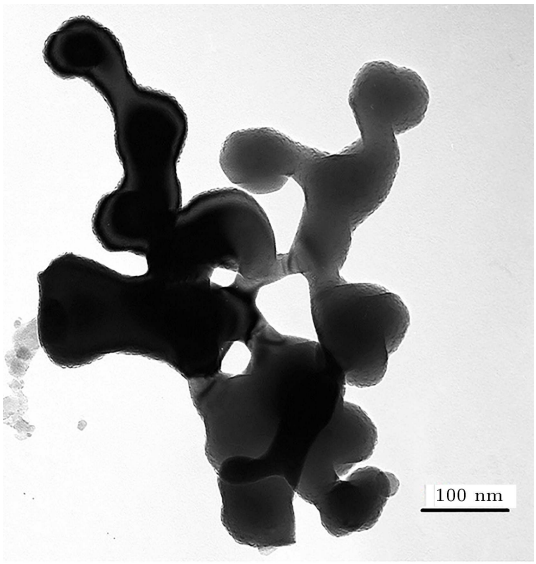

(a)

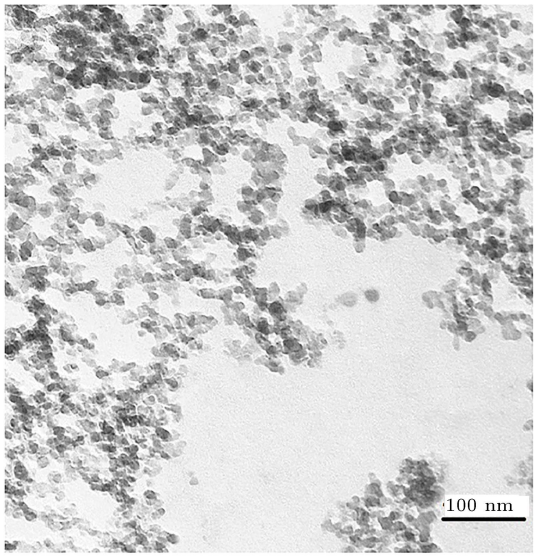

(b)

Figure 5. Transmission Electron Microscopy (TEM) image of deionized water-based nanoparticles at a volumetric concentration of 0.5%: (a) Al_2O_3 and (b) SiO_2.

on to apply heat flux to the surface and the fluid. For this purpose, the voltage of the power supply increases step by step until the boiling process reaches the CHF. After each step of increasing voltage and reaching a steady state, the temperature of the thermocouples is recorded by TM4-type thermostat to predict surface temperature and heat flux. In the present study, the steady state (temperature change of thermocouples less than 0.1°C) is achieved less than 15 minutes in all experiments. After reaching the CHF, due to the lack of contact of the cooling fluid with the boiling surface, a sudden jump in temperatures is observed which is recorded by the thermocouples and the turbulence of the fluid under boiling process is reduced. An unstable

vapor layer covers the surface and the boiling occurs in a transient manner. In this step, although the operating voltage does not increase, the temperature of the thermocouples continues to increase. In order to observe and evaluate the stable film boiling, the surface temperature must be sufficiently high. Therefore, the boiling process after CHF is allowed to reach the highest thermocouple temperature of about 400°C. Then, the applied voltage decreases in order to limit the temperature rise of the thermocouples. In this step, through trial and error (decreasing and increasing voltage), the operating voltage is changed to keep the temperature of thermocouples almost constant. In the next step, the temperature of the thermocouples must remain high so that the boiling process is stable in the film boiling region (point A in Figure 6). Upon reaching steady state, the applied voltage is reduced in a stepwise manner until the film boiling process reaches the MHF and the hysteresis curve of the film boiling can be plotted according to the schematic diagram of Figure 6 [23].

Figure 7 schematically shows the location of the thermocouples in the copper cartridge. As shown in Figure 7, T_1, T_2, and T_3 represent the thermocouple temperatures of 1, 2, and 3, respectively, and T_s represents the surface temperature.

With proper insulation around the copper cartridge, radial heat transfer to the environment can be neglected and heat transfer is considered as one dimensional along the cartridge. Therefore, with respect to the thermal conductivity of copper, the temperature of the thermocouples, and the distance between the holes embedded in the cartridge, the heat flux can be calculated using Eq. (2):

$$q'' = -k\frac{T_3 - T_1}{\Delta Z_{1-3}}. \tag{2}$$

In Eq. (2), ΔZ_{1-3} is the distance between Thermocouples 1 and 3. If the heat flux is known, the Fourier law can be used to predict the surface temperature at any constant heat flux according to Eq. (3):

$$T_s = T_1 - \frac{q''\Delta Z_{s-1}}{k}, \tag{3}$$

where ΔZ_{s-1} is the distance between the boiling surface and Thermocouple 1. The boiling heat transfer coefficient can be calculated using Eq. (4):

$$h = \frac{q''}{(T_s - T_{sat})}. \tag{4}$$

Figures 8 and 9 shows the temperature change diagram of the three thermocouples in four different fluxes according to their position on the cartridge in the nucleate and film boiling regimes, respectively, to keep one-dimensional heat transfer assumption. According to these figures, through the least squares method, the deviation for nucleate boiling is greater than 0.99

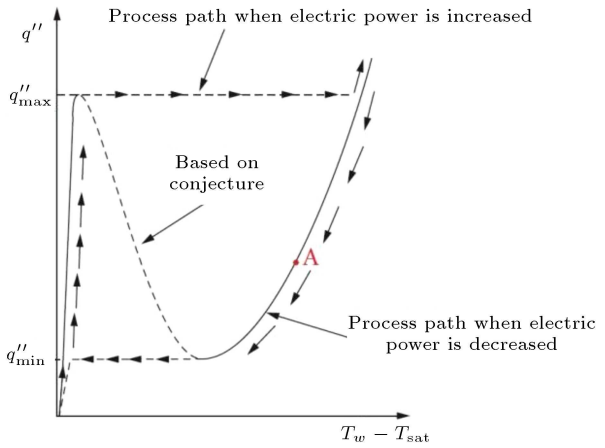

Figure 6. Schematic of the pool boiling curve [23].

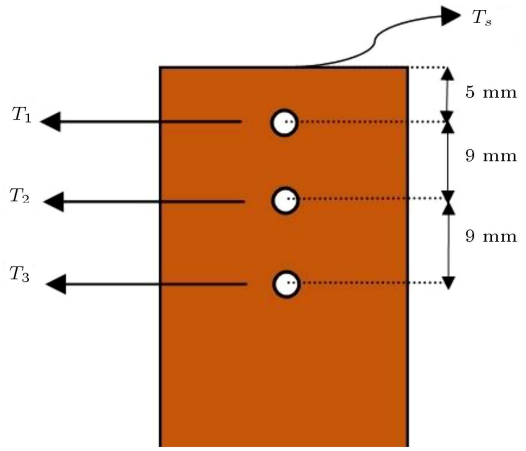

Figure 7. Schematic of the location of the thermocouples in the copper cartridge.

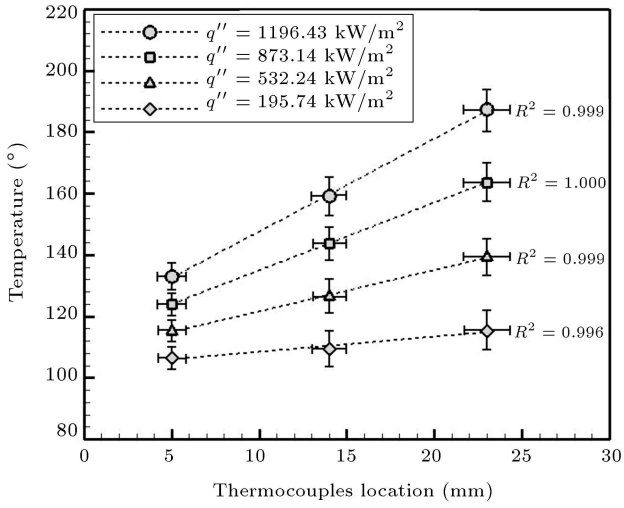

Figure 8. Linear temperature variations of thermocouples depending on their location on the cartridge for nucleate boiling.

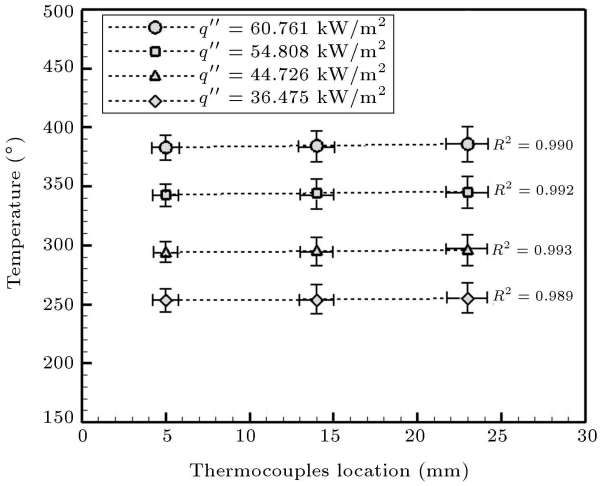

Figure 9. Linear temperature variations for thermocouples depending on their location on the cartridge for film boiling.

Table 3. Experimental data uncertainty.

Parameter	Uncertainty
Thermocouples temperature (°C)	±0.1
Voltage (V)	±1%
Current (I)	±0.1%
CNC machining (mm)	±0.1

and for film boiling greater than 0.98. Therefore, one-dimensional heat transfer is assumed correct, but there is always some loss in some part of the heat generated in the elements.

Table 3 presents data uncertainty in the present research experiments. It is necessary to explain that the holes of the thermocouples located in the copper block were produced by CNC numerical control machining.

The assumption that the thermal conductivity of copper remains constant during the test may cause error in the test results and, therefore, its uncertainty needs to be calculated. The thermal conductivities of copper at 100°C and 300°C are 395.89 W/m.°C and 382.89 W/m.°C, respectively [24]. In nucleate boiling experiments, the thermal conductivity of copper is considered constant and its uncertainty is 3.28%. Because of the significant surface temperature variations in the film boiling experiments, variations in the thermal conductivity of copper are not negligible and the value for each temperature is interpolated from the reference tables [24] with the maximum uncertainty being 0.063%.

In the present study, Moffat method [25] was employed to calculate heat flux, surface, and fluid temperature difference and boiling heat transfer coefficient uncertainties.

As shown by the Fourier heat conduction relation, the magnitude of the heat flux error depends on the thermal conductivity errors of the copper, temperatures, and location of the thermocouples according to Eq. (5). Therefore, the heat flux uncertainty can be calculated from Eq. (6) using Moffat method:

$$q'' = f(k, \Delta T, \Delta Z), \tag{5}$$

$$\frac{U_{q''}}{q''} = \sqrt{\left(\frac{U_{T_3-T_1}}{T_3-T_1}\right)^2 + \left(\frac{U_{Z_3-Z_1}}{Z_3-Z_1}\right)^2 + \left(\frac{U_k}{k}\right)^2}. \tag{6}$$

Eq. (7) can be used to calculate the uncertainty of the surface and fluid temperature difference (ΔT_s):

$$\frac{U_{\Delta T_s}}{\Delta T_s} = \sqrt{\left(\frac{U_{T_1-T_{sat}}}{T_1-T_{sat}}\right)^2 + \left(\frac{U_{Z_1}}{Z_1}\right)^2 + \left(\frac{U_k}{k}\right)^2}. \tag{7}$$

Eq. (8) can be used to calculate the uncertainty of the boiling heat transfer coefficient:

$$\frac{U_h}{h} = \sqrt{\left(\frac{U_{q''}}{q''}\right)^2 + \left(\frac{U_{\Delta T_s}}{\Delta T_s}\right)^2}. \tag{8}$$

Table 4 presents the heat flux, the surface and fluid temperature differences, and the boiling heat transfer coefficient uncertainties. Based on the accuracy of the measuring instruments, the maximum errors in calculating the heat flux and the heat transfer coefficient of the nucleate boiling were 8.6% and 9.7%, respectively. In addition, they were 11.7% and 11.9% in the calculation of heat flux and heat transfer coefficient of the film boiling, respectively.

3. Validation of results

In the present study, laboratory data were validated for both nucleate and film boiling regimes. For this purpose, the nucleate boiling data obtained from

Table 4. Uncertainty of parameters in nucleate and film boiling.

Parameter	Uncertainty in nucleate boiling (%)	Uncertainty in film boiling (%)
Heat flux (kW/m^2)	±8.6	±11.7
Surface and fluid temperature differences (°C)	±4.5	±2
Heat transfer coefficient (kW/m^2.°C)	±9.7	±11.9

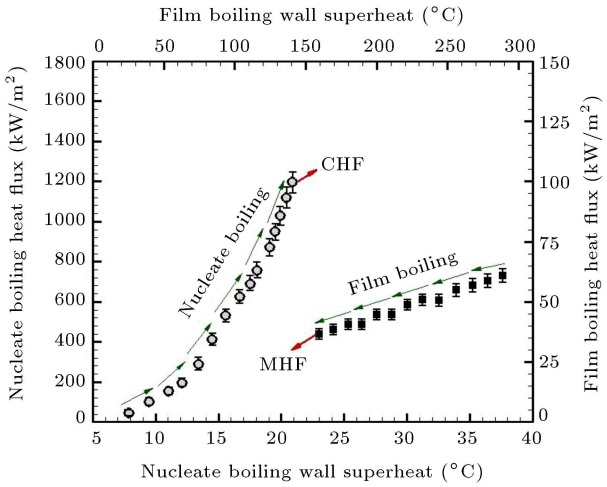

Figure 10. Heat flux curve versus wall superheat temperature difference for nucleate and film boiling of deionized water on the polished copper surface.

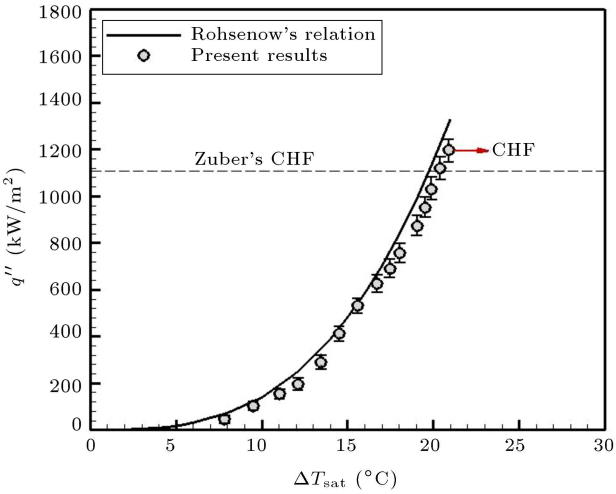

Figure 11. Comparison of the nucleate boiling curve of the present study and the Rohsenow experimental relationship.

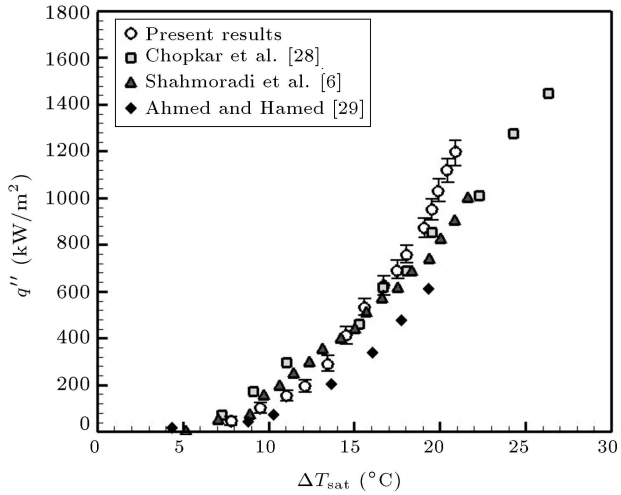

Figure 12. Comparison between the nucleate boiling curve of the present study and the results of other researchers.

the experiments were compared with the empirical relationships and the results of other researchers. In addition, the film boiling data obtained from the experiments were compared with valid experimental relationships. Finally, a repeatability test was performed to complete the verification.

Before conducting the experiments, the copper surface was polished by 1500 grain sanding to create a smooth boiling surface. After surface preparation, experiments were performed using deionized water as the working fluid on the polished surface.

In Figure 10, the heat flux diagram is plotted versus the wall superheat temperature difference using the data of the deionized water boiling experiment on the polished copper surface.

Using the Rohsenow empirical relation [26], the heat flux of nucleate boiling can be calculated in terms of the wall superheat temperature difference according to Eq. (9):

$$\left[\frac{c_{pl}\Delta T_{sat}}{i_{lv}}\right] = C_{sf}\left[\frac{q''}{\mu_l i_{lv}}\sqrt{\frac{\sigma}{g(\rho_l-\rho_v)}}\right]^n \left[\frac{c_p\mu}{k}\right]_l^{m+1}. \quad (9)$$

In Eq. (9), c_{pl}, μ_l, k, and ρ_l are the specific heat capacity, dynamic viscosity, thermal conductivity, and liquid density, respectively, ρ_v is the vapor density, i_{lv} the latent heat of evaporation, and σ the surface tension. For boiling the water, $n = 0.33$, $m = 0$, and surface-fluid correction coefficient for water-Cu composition is $C_{sf} = 0.013$. Using Zuber empirical relation [27], the CHF for pure deionized water can be calculated through Eq. (10):

$$q''_{\max} = 0.131 i_{lv}\rho_v^{0.5}[\sigma g(\rho_l-\rho_v)]^{0.25}. \quad (10)$$

In Figure 11, the nucleate boiling curve of the present study is compared with the Rohsenow empirical relation, which has a maximum error of 9.7%. As shown in Figure 11, the Rohsenow relation agrees satisfactorily with the data of the present experiments. Using the Zuber empirical relation, the CHF for pure deionized water is 1108 kW/m^2, which has 7.9% error compared to the CHF in the present study.

In Figure 12, the nucleate boiling curve of the present study is compared with the results of other researchers [6,28,29]. As shown in Figure 12, the data of the present experiments have good agreement with other empirical data.

Berenson [30] by combining the theory of wave hydrodynamic instability with Bromley's model [31], has proposed an experimental relation for film boiling on a horizontal flat plate. proposed an experimental relation for film boiling on a horizontal flat plate. Upon using it, the heat transfer coefficient of the film boiling

(h_{fb}) can be calculated in terms of the wall superheat temperature difference (ΔT_{sat}) according to Eq. (11):

$$h_{fb} = 0.425 \left[\frac{k_v^3 \rho_v \Delta\rho g i'_{lv}}{\mu_v \Delta T_{sat} \sqrt{\sigma / g(\Delta\rho)}} \right]^{\frac{1}{4}}. \quad (11)$$

In Eq. (11), i'_{lv} is the effective latent heat of evaporation which can be calculated using Eq. (12):

$$i'_{lv} = i_{lv} \left[1 + 0.5 \left(\frac{c_{pv} \Delta T_{sat}}{i_{lv}} \right) \right]. \quad (12)$$

Using the Berenson empirical relations, the MHF and the wall superheat temperature difference of the film boiling starting point ($\Delta T_{\min}$) can be calculated. Because the steam properties are implicitly dependent on temperature, the iteration method is used:

$$q''_{\min} = 0.091 \rho_v i_{lv} \left[\frac{\sigma g \Delta\rho}{(\rho_l + \rho_v)^2} \right]^{\frac{1}{4}}, \quad (13)$$

$$\Delta T_{\min} = \frac{q''_{\min}}{h_{fb}}. \quad (14)$$

Henry [32] proposed Eq. (15) by considering the effects of solid surface thermophysical properties on the minimum film boiling temperature:

$$\frac{T_{\min} - T^*_{\min}}{T^*_{\min} - T_l} = 0.42 \left[\sqrt{\frac{(\rho c k)_f}{(\rho c k)_w}} \frac{i_{lv}}{C_w (T^*_{\min} - T_{sat})} \right]^{0.6}. \quad (15)$$

In Eq. (15), $T^*_{\min}$ is the minimum film boiling temperature, which is obtained by the Berenson relation. The index f is for saturated liquid and w for solid surface.

In Figure 13, the film boiling heat transfer coefficient of the present study is compared with the Berenson empirical relation, which has a maximum error of 10.7%.

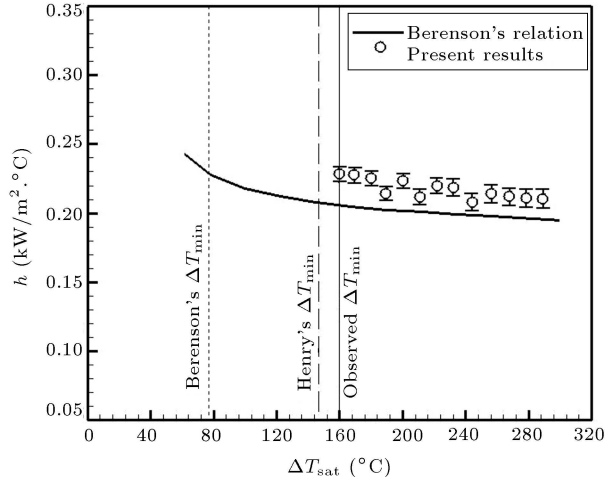

Figure 13. Comparison of the film boiling heat transfer coefficient curve of the present study and the Berenson empirical relation.

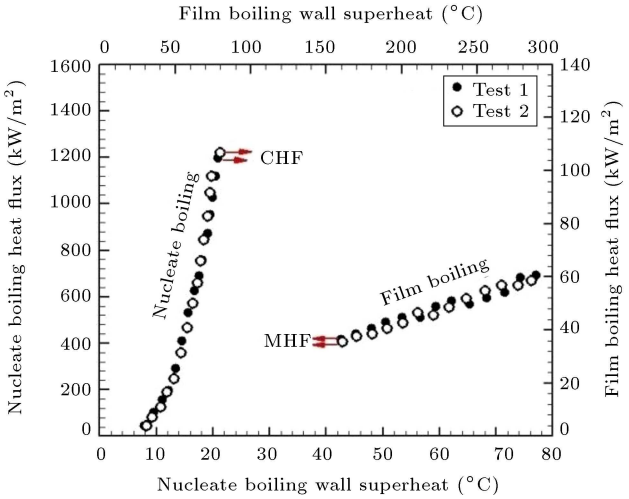

Figure 14. Repeatability of pure deionized water nucleate and film boiling on the polished copper surface.

By using Berenson empirical relations, $\Delta T_{\min}$ is obtained as 77.02°C for pure deionized water. Upon using the Henry relation and considering the effects of the thermophysical properties of copper, $\Delta T_{\min}$ is obtained as 146°C. In the present study, $\Delta T_{\min}$ for pure deionized water on a polished cooper surface is obtained as 159.7°C, which differs by 9.3% from the Henry empirical relation.

In order to investigate the repeatability test, pure deionized water boiling experiments were performed on the polished copper surface on two different days and the nucleate and film boiling diagrams are plotted in Figure 14. The amount of error in the CHF is 1.9% and in the MHF is 2.8%, which indicates the accuracy of the results.

Figure 15 shows how bubbles form on the polished copper surface at different heat fluxes. At low heat fluxes (Figure 15(a)), the bubbles are smaller and as the heat flux increases, the small bubbles merge to form larger bubbles (Figure 15(b) to (f)). After CHF and the transient boiling region, a layer of stable steam coats the surface and the film boiling occurs (Figure 15(h)).

4. Results

4.1. Nucleate boiling results

In the present experiments, the CHF value of pure deionized water is 1196.43 kW/m^2, which occurs at a wall superheat temperature difference of 20.89°C. In addition, maximum nucleate boiling heat transfer coefficient of pure deionized water is 57.27 kW/m^2.°C.

Figure 16 plots the deionized water-based nanofluids Al_2O_3 and SiO_2 with three volumetric concentrations of 0.1%, 0.3%, and 0.5% and pure deionized water nucleate boiling curve. As shown in Figure 16, CHF of Al_2O_3 nanofluid occurs at higher wall superheat temperature difference than pure deionized water such

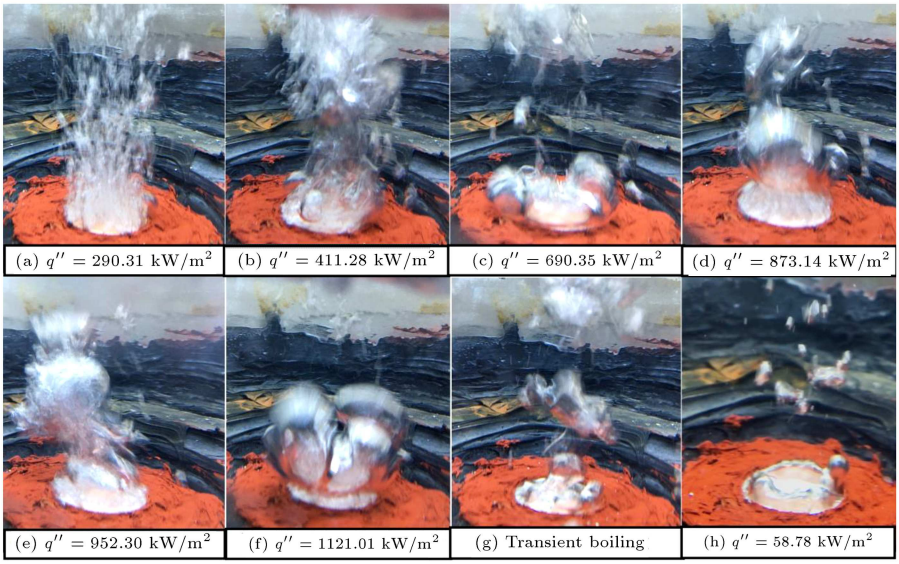

Figure 15. Bubble formation and vapor film on the polished copper surface.

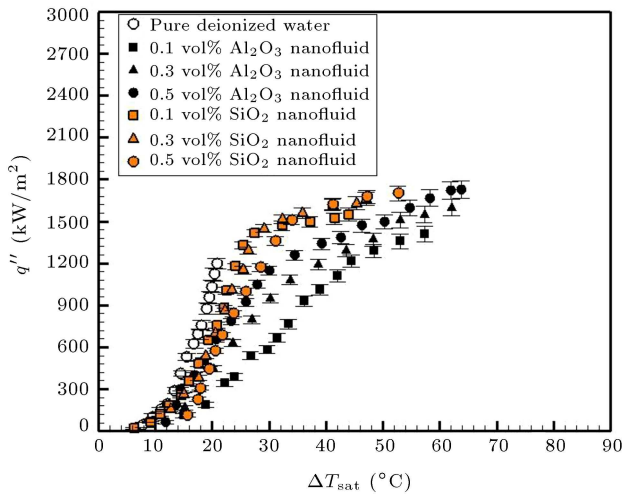

Figure 16. Nucleate boiling curve for Al_2O_3 and SiO_2 deionized water-based nanofluids at different volumetric concentrations.

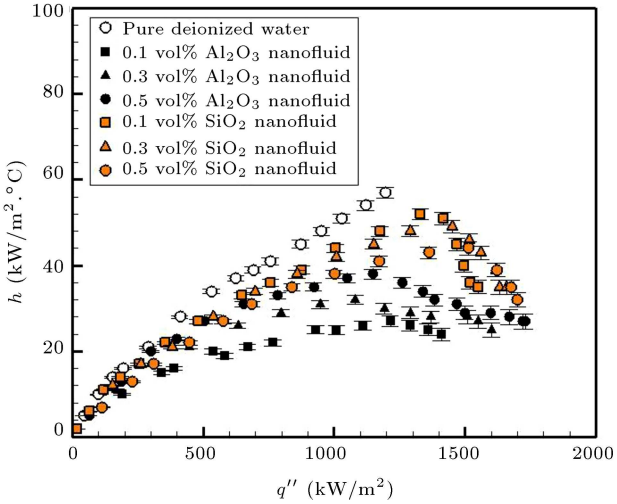

Figure 17. Nucleate boiling heat transfer coefficient versus heat flux for Al_2O_3 and SiO_2 deionized water-based nanofluids with different volumetric concentrations.

that ΔT_{sat} for volumetric concentrations of 0.1%, 0.3%, and 0.5% is 57.4°C, 62.1°C, and 63.8°C, respectively. The presence of Al_2O_3 nanoparticles in the deionized water-based nanofluid increases the CHF so that its values for volumetric concentrations of 0.1%, 0.3%, and 0.5% are 1410 kW/m^2, 1600.5 kW/m^2, and 1729.6 kW/m^2, respectively. Figure 16 indicates that the presence of SiO_2 nanoparticles in the deionized water-based nanofluid has delayed the integration of bubbles into each other and significantly increased the wall superheat temperature difference at which the CHF occurs. Therefore, the CHFs for volumetric concentrations of 0.1%, 0.3%, and 0.5% are associated with wall superheat temperature difference of 44°C, 47.1°C, and 52.7°C, respectively. The CHF values for SiO_2 nanofluid with volumetric concentrations of 0.1%, 0.3%, and 0.5% are 1550.42 kW/m^2, 1660.35 kW/m^2, and 1701.27 kW/m^2, respectively.

In Figure 17, the nucleate boiling heat transfer coefficient of Al_2O_3 and SiO_2 deionized water-based nanofluids with three volumetric concentrations of 0.1%, 0.3%, and 0.5% is plotted versus the heat flux. As shown in Figure 17, at a constant heat flux, the nucleate boiling heat transfer coefficient of Al_2O_3 and SiO_2 nanofluids is reduced compared to pure deionized water. At higher heat fluxes, there is a further reduction due to the deposition of nanoparticles on the boiling surface. As the volumetric concentration of Al_2O_3 nanofluid increases from 0.1% to 0.5%, the heat transfer coefficient of the nucleate boiling increases.

Maximum nucleate boiling heat transfer coefficient of Al_2O_3 deionized water-based nanofluid for volumetric concentrations of 0.1%, 0.3%, and 0.5% is 27.30 kW/m^2.°C, 32.10 kW/m^2.°C, and 38.26 kW/m^2.°C, respectively. Unlike Al_2O_3 nanofluid, the nucleate boiling heat transfer coefficient of SiO_2 deionized water-based nanofluid decreases with increasing volumetric concentration from 0.1% to 0.5%. Maximum nucleate boiling heat transfer coefficient of SiO_2 deionized water-based nanofluid for volumetric concentrations of 0.1%, 0.3%, and 0.5% is 52.15 kW/m^2.°C, 49.83 kW/m^2.°C, and 44.53 kW/m^2.°C, respectively.

In this section, the results of the nucleate boiling of the nanofluids with three different volumetric concentrations on the polished copper surface are summarized and compared with the results of pure deionized water. The results showed that for both nanofluids with all volumetric concentrations, the CHF occurs at a higher wall superheat temperature difference than that of pure deionized water. In addition, in all cases, the presence of nanoparticles in the base fluid improves the CHF. The boiling of Al_2O_3 deionized water-based nanofluid with a volumetric concentration of 0.5% had the highest CHF, with an increase of 44.56% compared to pure deionized water. The SiO_2 deionized water-based nanofluid with a volumetric concentration of 0.5% had the best performance among the two other concentrations so that the CHF value increased by 42.19% compared to pure deionized water.

In nanofluid boiling, two phenomena including:

(a) Increased heat transfer due to increased thermal conductivity, convection, and fluid turbulence;

(b) Reduced heat transfer due to closure of surface holes by nanoparticles and small number of nucleation sites.

The results of the present study show that in nucleate boiling, the increased effect of heat transfer is dominated by its reduced effect and for both nanoparticles at all volumetric concentrations, the heat transfer coefficient of nucleate boiling is reduced compared to pure deionized water. The value for this reduction was greater for Al_2O_3 nanofluid than that for SiO_2 nanofluid because the size of Al_2O_3 nanoparticles was larger and their deposition on the boiling surface was more significant.

4.2. Film boiling results

In the present experiments, the MHF value of pure deionized water is 36.48 kW/m^2, which occurs at a wall superheat temperature difference of 159.7°C. In addition, the maximum film boiling heat transfer coefficient of pure deionized water is 0.228 kW/m^2.°C.

Figure 18 plots the deionized water-based nanofluids Al_2O_3 and SiO_2 with three volumetric concentrations of 0.1%, 0.3%, and 0.5% and pure deionized water film boiling curve. As shown in Figure 18, the presence of Al_2O_3 nanoparticles in the base fluid causes the starting point of stable film boiling to be at higher wall superheat temperature difference such that ΔT_{min} for volumetric concentrations of 0.1%, 0.3%, and 0.5% is 176.3°C, 172.5°C, and 170.7°C, respectively. By increasing the volumetric concentration of Al_2O_3 nanofluid from 0.1% to 0.5%, stable film boiling started with a lower wall superheat temperature difference. The MHF values for Al_2O_3 nanofluid with volumetric concentrations of 0.1%, 0.3%, and 0.5% are 44.92 kW/m^2, 47.09 kW/m^2, and 49.25 kW/m^2, respectively, which increase compared to pure deionized water. Similar to Al_2O_3 nanoparticles, the presence of SiO_2 nanoparticles in the base fluid causes the starting point of stable film boiling to be at higher wall superheat temperature difference such that ΔT_{min} for volumetric concentrations of 0.1%, 0.3%, and 0.5% is 172.4°C, 177.4°C, and 179.9°C, respectively. Unlike Al_2O_3 nanofluid, in SiO_2 nanofluid with increasing the volumetric concentration from 0.1% to 0.5%, stable film boiling begins at higher wall superheat temperature differences. The MHF values for SiO_2 nanofluid with volumetric concentrations of 0.1%, 0.3%, and 0.5% are 42.81 kW/m^2, 47.05 kW/m^2, and 49.03 kW/m^2, respectively, which increased compared to pure deionized water.

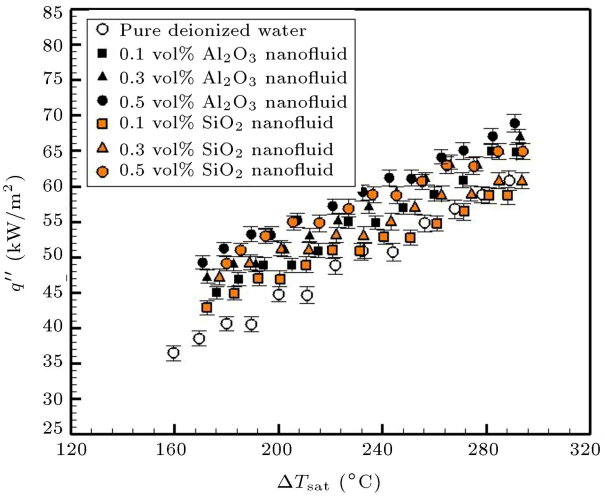

Figure 18. Film boiling curve for Al_2O_3 and SiO_2 deionized water-based nanofluids at different volumetric concentrations.

Figure 19 plots the film boiling heat transfer coefficient of Al_2O_3 and SiO_2 deionized water-based nanofluids with three volumetric concentrations of 0.1%, 0.3%, and 0.5% versus wall superheat temperature difference. According to Figure 19, for Al_2O_3 nanofluid in all the three volumetric concentrations, the film boiling heat transfer coefficient at a constant wall superheat temperature difference increased compared to pure deionized water. The value of this

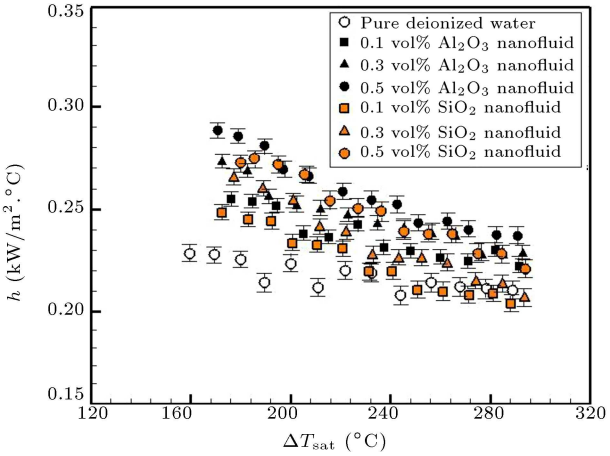

Figure 19. Film boiling heat transfer coefficient versus wall superheat temperature difference for Al_2O_3 and SiO_2 deionized water-based nanofluids with different volumetric concentrations.

increment is more evident at the lower wall superheat temperature differences. Maximum film boiling heat transfer coefficient of Al_2O_3 deionized water-based nanofluid for volumetric concentrations of 0.1%, 0.3%, and 0.5% is 0.255 kW/m^2.°C, 0.273 kW/m^2.°C, and 0.288 kW/m^2.°C, respectively.

Figure 19 indicates that the presence of SiO_2 nanoparticles improves the heat transfer coefficient of the film boiling compared to pure deionized water. However, similar to Al_2O_3 nanoparticles with increase in the wall superheat temperature difference, the positive effects of the presence of SiO_2 nanoparticles on the heat transfer coefficient of film boiling are reduced. Maximum film boiling heat transfer coefficient of SiO_2 deionized water-based nanofluid for volumetric concentrations of 0.1%, 0.3%, and 0.5% is 0.248 kW/m^2.°C, 0.265 kW/m^2.°C, and 0.275 kW/m^2.°C, respectively.

In this section, the results of the film boiling of the nanofluids with three different volumetric concentrations on the polished copper surface are summarized and compared with those of pure deionized water. The outcome illustrated that for both nanofluids and all volumetric concentrations, stable film boiling begins at a higher wall superheat temperature difference than pure deionized water, due to the change in surface hydrophilicity induced by the nanoparticle deposition during boiling. Among the experiments in the present study, the highest MHF was related to Al_2O_3 deionized water-based nanofluid with a volumetric concentration of 0.5% and with an increase of 35.01% compared to pure deionized water. In SiO_2 deionized water-based nanofluid, the volumetric concentration of 0.5% had the best performance among the two other concentrations and the MHF increased by 34.40% compared to pure deionized water. For both nanofluids, the film boiling heat transfer coefficient increases compared to pure deionized water.

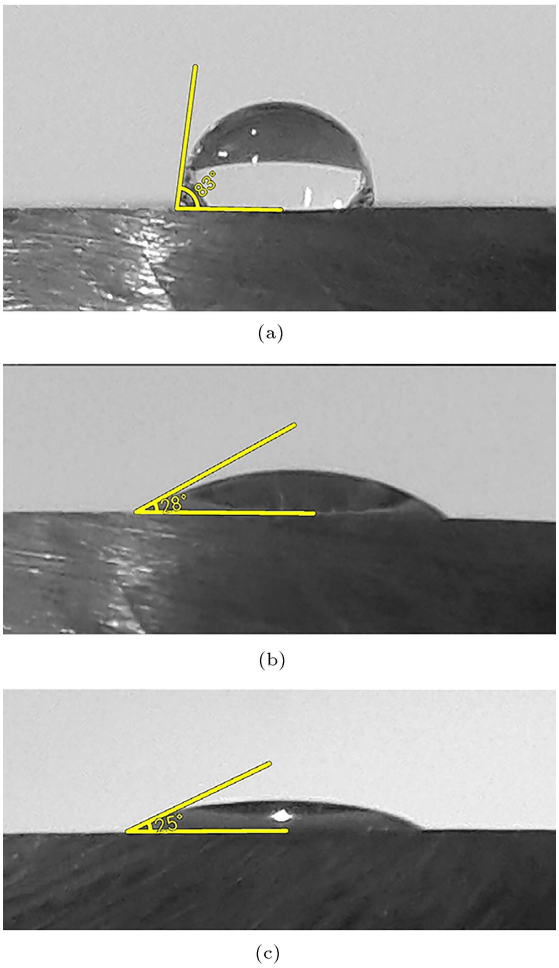

Figure 20. The static contact angle of the water droplet on the surface: (a) Before boiling, (b) after SiO_2 deionized water-based nanofluid boiling, and (c) after Al_2O_3 deionized water-based nanofluid boiling.

Droplet test was performed to investigate the variation of surface hydrophilicity after the boiling of nanofluids. Figure 20 shows the contact angle of the water droplet and the surface before the boiling and after the boiling of the nanofluids. Droplet test revealed that the nanoparticle deposition on the boiling surface made the boiling surface more hydrophilic. According to Figure 20, the contact angle of the water droplet and the surface before boiling is 83°. After nanofluid boiling and the nanoparticle deposition on the surface, the contact angle of the water droplet and the surface decreased sharply so that the values for the deposited surfaces by the Al_2O_3 and SiO_2 nanoparticles were 25° and 28°, respectively. As the surface becomes more hydrophilic, the droplet spreads rapidly to the surface; thereby filling and inactivating the nucleation sites by fluid and reducing the heat transfer coefficient of nucleate boiling. The more hydrophilic the surface, the greater the size and the time of bubble growth, resulting in a lower bubble separation frequency, thus delaying the occurrence of CHF and MHF. In film

boiling, the surface temperature is so high that a stable vapor layer forms on the boiling surface which causes no contact between liquid and solid. Thus, heat transfer is accomplished mainly by conduction and convection through the vapor film. Lack of direct solid-liquid contact prevents nucleation sites from being filled and inactivated by liquid droplets. In other words, in film boiling, surface hydrophilicity has no significant effect on filling the nucleation sites and destroying the bubbling process. For this reason, the factor involved in improving the thermal properties of nanofluids overcomes the destructive factor of inactivation of nucleation sites; thus, the heat transfer coefficient of film boiling increases.

5. Conclusion

In this paper, the nucleate and film boiling heat transfer characteristics of Al_2O_3 and SiO_2 deionized water-based nanofluids were studied experimentally. To this end, the nanofluids were prepared with three volumetric concentrations of 0.1%, 0.3%, and 0.5% and experiments were performed using pool boiling apparatus. It is noteworthy that the new results of nanofluid film boiling on the horizontal flat plate have been presented.

The nucleate boiling results showed that the addition of Al_2O_3 and SiO_2 nanoparticles to the base fluid reduced the heat transfer coefficient of the nucleate boiling. From this perspective, the addition of nanoparticles has led to a poor performance of nucleate boiling compared to pure deionized water. On the other hand, the Critical Heat Flux (CHF) of nanofluids at all three volumetric concentrations of 0.1%, 0.3%, and 0.5% was significantly higher than that of pure deionized water. For both Al_2O_3 and SiO_2 deionized water-based nanofluids, the CHF increased with increasing volumetric concentration. Therefore, from the perspective of the CHF, the addition of nanoparticles to the base fluid improved the performance of the boiling process.

The film boiling results showed that for both Al_2O_3 and SiO_2 deionized water-based nanofluids with three volumetric concentrations of 0.1%, 0.3%, and 0.5%, stable film boiling began at higher wall superheat temperature difference than pure deionized water. In addition, for both Al_2O_3 and SiO_2 deionized water-based nanofluids, as the volumetric concentration increased, the Minimum Heat Flux (MHF) increased. Due to the increase of the MHF and the occurrence of film boiling at higher wall superheat temperature difference for the nanofluids (compared to the base fluid), it can be concluded that adding nanoparticles to the base fluid improved the film boiling performance. It is interesting that nanofluids enhance the film boiling heat transfer coefficient. For both nanofluids, with increase in the volumetric concentration from 0.1% to 0.5%, the heat transfer coefficient of film boiling increased.

Nomenclature

C	Constant coefficient
c_p	Specific heat capacity (J/kg.°C)
g	Gravitational acceleration (m/s^2)
h	Boiling heat transfer coefficient (W/m^2.°C)
i	Latent heat of evaporation (J/kg)
k	Thermal conductivity (W/m.°C)
m	Mass (kg)
q''	Heat flux (W/m^2)
T	Temperature (°C)
U	Uncertainty
V	Volume (m^3)
Z	Thermocouples location in cartridge (m)
ΔT	Wall superheat (°C)
μ	Dynamic viscosity (kg/m.s)
ρ	Density (kg/m^3)
σ	Surface tension (N/m)
φ	Volumetric concentration of nanofluid

Subscripts

f	Saturated liquid
fb	Film boiling
l	Liquid
max	Maximum
min	Minimum
nf	Nanofluid
np	Nano particle
s	Boiling surface
sat	Saturation
sf	Solid-fluid
v	Vapor
w	Solid surface

Abbreviations

CHF	Critical Heat Flux (W/m^2)
MHF	Minimum Heat Flux (W/m^2)
PTFE	Polytetrafluoroethylene
TEM	Transmission Electron Microscopy

References

1. Rana, S., Nawaz, M., and Qureshi, I.H. "Numerical study of hydrothermal characteristics in nanofluid using KKL model with Brownian motion", *Sci. Iran.*, **26**(3), pp. 1931–1943 (2019).
2. Esmailpour, K., Azizi, A., and Hosseinalipour, S.M. "Numerical study of jet impingement subcooled boiling on superheated surfaces", *Sci. Iran.*, **26**(4), pp. 2369–2381 (2019).
3. Pournaderi, P. and Pishevar, A.R. "Numerical simulation of oblique impact of a droplet on a surface in the film boiling regime", *Sci. Iran.*, **21**(1), pp. 119–129 (2014).
4. Kamel, M.S., Al-agha, M.S., Lezsovits, F., et al. "Simulation of pool boiling of nanofluids by using Eulerian multiphase model", *J. Therm. Anal. Calorim.*, **142**, pp. 493–505 (2020).
5. An, Y.S. and Kim, B.J. "Numerical investigation of film boiling heat transfer on the horizontal surface in an oscillating system with low frequencies", *Nucl. Eng. Technol.*, **52**(5), pp. 918–924 (2020).
6. Shahmoradi, Z., Etesami, N., and Esfahany, M.N. "Pool boiling characteristics of nanofluid on flat plate based on heater surface analysis", *Int. Commun. Heat Mass Transf.*, **47**, pp. 113–120 (2013).
7. Raveshi, M.R., Keshavarz, A., Mojarrad, M.S., et al. "Experimental investigation of pool boiling heat transfer enhancement of alumina-water-ethylene glycol nanofluids", *Exp. Therm. Fluid Sci.*, **44**, pp. 805–814 (2013).
8. Umesh, V. and Raja, B. "A study on nucleate boiling heat transfer characteristics of pentane and CuO-pentane nanofluid on smooth and milled surfaces", *Exp. Therm. Fluid Sci.*, **64**, pp. 23–29 (2015).
9. Ji, W.T., Zhao, P.F., Zhao, C.Y., et al. "Pool boiling heat transfer of water and nanofluid outside the surface with higher roughness and different wettability", *Nanoscale Microscale Thermophys.*, **22**(4), pp. 296–323 (2018).
10. Dareh, F.R., Haghshenasfard, M., Esfahany, M.N., et al. "An experimental investigation of pool boiling characteristics of alumina-water nanofluid over micro/nano-structured surfaces", *Heat Transfer Eng.*, **40**(20), pp. 1691–1708 (2019).
11. Kiyomura, I.S., Manetti, L.L., da Cunha, A.P., et al. "An analysis of the effects of nanoparticles deposition on characteristics of the heating surface and on pool boiling of water", *Int. J. Heat Mass Transf.*, **106**, pp. 666–674 (2017).
12. Vasudevan, D., Senthilkumar, D., and Surendhiran, S. "Performance and characterization studies of reduced graphene oxides aqua nanofluids for a pool boiling surface", *Int. J. Thermophys.*, **41**, p. 74 (2020).
13. Reddy, Y.A. and Venkatachalapathy, S. "Heat transfer enhancement studies in pool boiling using hybrid nanofluids", *Thermochim. Acta*, **672**, pp. 93–100 (2019).
14. Kamel, M.S. and Lezsovits, F. "Experimental investigation on pool boiling heat transfer performance using tungsten oxide WO_3 nanomaterial-based water nanofluids", *Materials*, **13**(8), p. 1922 (2020).
15. Mohammadi, M. and Khayat, M. "Experimental investigation of the effect of one-dimensional roughened surface on the pool boiling of nanofluids", *Sci. Iran.*, **27**(6), pp. 2954–2966 (2020).
16. Gylys, J., Skvorcinskiene, R., Paukstaitis, L., et al. "Film boiling influence on the spherical body's cooling in sub-cooled water", *Int. J. Heat Mass Transf.*, **95**, pp. 709–719 (2016).
17. Arai, T. and Furuya, M. "Effect of nanofluid on the film boiling behavior at vapor film collapse", *17th Int. Conf. Nucl. Eng.*, Brussels, Belgium (2009).
18. Ciloglu, D., Bolukbasi, A., and Comakli, K. "Effect of nanofluids on the saturated pool film boiling", *World Acad. Sci. Eng. Technol.*, **6**(7), pp. 1112–1124 (2012).
19. Li, J.Q., Fan, L.W., Zhang, L., et al. "An Experimental study of boiling heat transfer during quenching of nanofluids with carbon nanotubes of various sizes", *ASME Heat Transfer Summer Conf.*, Washington, DC, USA (2016).
20. Kang, J.Y., Kim, T.K., Lee, G.C., et al. "Minimum heat flux and minimum film-boiling temperature on a completely wettable surface: Effect of the Bond number", *Int. J. Heat Mass Transf.*, **120**, pp. 399–410 (2018).
21. Wciślik, S. "A simple economic and heat transfer analysis of the nanoparticles use", *Chem. Pap.*, **71**(12), pp. 2395–2401 (2017).
22. Talari, V., Behar, P., Lu, Y., et al. "Leidenfrost drops on micro/nanostructured surfaces", *Front Energy.*, **12**(1), pp. 22–42 (2018).
23. Ghiaasiaan, S.M., *Two Phase Flow, Boiling and Condensation in Conventional and Miniature Systems*, Cambridge University Press, New York (2008).
24. Hust, J.G. and Lankford, A.B., *Thermal Conductivity of Aluminum, Copper, Iron, and Tungsten for Temperatures From 1 K to the Melting Point*, U.S. Department of Commerce, Malcolm Baldrige, Colorado (1984).
25. Moffat, R.J. "Describing the uncertainties in experimental results", *Exp. Therm. Fluid Sci.*, **1**(1), pp. 3–17 (1988).
26. Rohsenow, W.M. "A method of correlating heat transfer data for surface boiling liquids", *Trans. ASME.*, **74**, pp. 969–975 (1952).
27. Zuber, N. "On the stability of boiling heat transfer", *Trans. ASME.*, **80**, pp. 711–720 (1958).

28. Chopkar, M., Das, A.K., Manna, I., et al. "Pool boiling heat transfer characteristics of ZrO_2-water nanofluids from a flat surface in a pool", *Heat Mass Transf.*, **44**(8), pp. 999–1004 (2008).

29. Ahmed, O. and Hamed, M.S. "Experimental investigation of the effect of particle deposition on pool boiling of nanofluids", *Int. J. Heat Mass Transf.*, **55**(13–14), pp. 3423–3436 (2012).

30. Berenson, P.J. "Film-boiling heat transfer from a horizontal surface", *J. Heat Transf.*, **83**, pp. 351–356 (1961).

31. Bromley, L.A. "Heat transfer in stable film boiling", *Chem. Eng. Prog. Symp. Ser.*, **46**, pp. 221–227 (1950).

32. Henry, R.E. "A correlation for the minimum film boiling temperature", *Chem. Eng. Prog. Symp. Ser.*, **70**(138), pp. 81–90 (1974).

Biographies

Seyed Hadi Golkar is currently a PhD student at the Department of Mechanical Engineering at Science and Research Branch, Islamic Azad University, Tehran, Iran. His major interest areas are heat and mass transfer, energy conversion, and multiphase flow.

Morteza Khayat is an Assistant Professor at the Department of Mechanical Engineering at Science and Research Branch, Islamic Azad University, Tehran, Iran. He obtained his PhD degree in Mechanical Engineering from Sharif University of Technolog (SUT), Tehran, Iran. His major interest areas are multiphase flow, heat transfer in porous media, and non-Newtonian fluid flow.

Masoud Zareh is an Assistant Professor at the Department of Mechanical Engineering at Science and Research Branch, Islamic Azad University, Tehran, Iran. He received his PhD degree in Mechanical Engineering and Energy Conversion from Islamic Azad University. His research interest area includes two-phase flow and heat transfer, pulsating and oscillating heat pipes, Computational Fluid Dynamics (CFD), and modeling and simulation of transport phenomena in porous media.